INTERNATIONAL JOURNAL OF HYDROGEN ENERGY 46 (2021) 22574–22590

Available online at www.sciencedirect.com

ScienceDirect

journal homepage: www.elsevier.com/locate/he

Review Article

Critical review of models for H_2-permeation through polymers with focus on the differential pressure method☆

Johannes Macher[*], *Andreas Hausberger*, *Astrid E. Macher*, *Matthias Morak*, *Bernd Schrittesser*

Polymer Competence Center Leoben GmbH, Roseggerstraße 12, A-8700 Leoben, Austria

HIGHLIGHTS

- Review of models for single- and multi-layered membrane permeation.
- Recommendation of curve fitting instead of time lag or flow rate measurements.
- Empirical equations of state for viscosity and density of hydrogen.
- Discussion of the influence of porous plates on permeation measurements.

ARTICLE INFO

Article history:
Received 15 December 2020
Received in revised form
13 April 2021
Accepted 16 April 2021
Available online 24 May 2021

Keywords:
Hydrogen
Polymer
Single-layer
Multi-layer
Modelling
Review

ABSTRACT

To reduce loss of hydrogen in storage vessels with high energy-to-weight-ratio, new materials, especially polymers, have to be developed as barrier materials. Very established methods for characterization of barrier materials with permeation measurements are the time-lag and flow rate method along with the differential pressure method, which resembles the nature of hydrogen vessel systems very well. Long measurement durations are necessary to gain suitable measurement data for these evaluation methods, and often restrictive conditions have to be fullfilled. For these reasons, common models for hydrogen permeation through single-layer and multi-layer membranes, as well as models for hydrogen gas properties were collected and reviewed. Using current computer power together with these models can reduce measurement time for characterization of the barrier properties of materials, while additional information about the quality of the measurement results is obtained.

☆ This document is one result of the research project "Polymers4Hydrogen" (project-no.: 872165) funded by the Austrian Government.
* *Corresponding author.*
E-mail address: johannes.macher@pccl.at (J. Macher).
http://dx.doi.org/10.1016/j.ijhydene.2021.04.095

Contents

Nomenclature

$\Delta\eta(\rho, T)$	Excess viscosity
η	Viscosity of fluid/gas
$\eta_0(T)$	Viscosity at the limit $\rho = 0$
$\widehat{v}$, $\widehat{f}$	Non-dimensionalized variable, reduced function
λ_n, λ_m	Eigenvalues of spatial eigenfunctions
$\Omega_\eta(T)$	Collision integral
φ	Porosity of a material
ρ	(Gas) density
σ, ϵ/k_B	Lennard-Jones parameters
τ	Time variable, dimensionless
$\widetilde{T}_n(t)$	Temporal eigenfunctions for membrane
$\widetilde{X}_n(x)$	Spatial eigenfunctions for membrane
A	Area, cross-sectional
a_i, b_i, c_i	Constants for the calculation of the compressibility factor $Z(p, T)$ for hydrogen
b_n, b_m	Constant coefficients of the infinite sums in the transient solution in the material/layer
C, C_i	Concentration in material/layer
C_1, C_2	Constant boundary conditions of the concentration distribution
$C_{b\pm}$	Intermediate concentration values on interface between layers
$C_{j\pm n}$	Concentration at grid points
D, D_i	Diffusion constant of material/layer
$F(t)$	Flux (density) out of membrane
$F_A(t)$	Flux out of membrane dependent on area
G_m	Constant of the multi-layer transient solution which is independent of x and t
H, H_n	Constant of the single-layer transient solution which is independent of x and t
h_i	Spacings of numerical grid
$J_{i,m}$	Constant of the multi-layer transient solution which is independent of x and t
k_B	Boltzmann constant
K_D	Darcy permeability
K_F	Forchheimer constant, inertial factor
$K_{i,m}$	Constant of the multi-layer transient solution which is independent of x and t
L, L_i	Thickness of membrane/layer
M, M_n	Constant of the single-layer transient solution which is independent of x and t
O, O_n	Constant of the single-layer transient solution which is independent of x and t
o_i, u_i, s_i	Constants for the calculation of hydrogen gas viscosity
p, p_i	Pressure, pressures at specific locations
Pe	Permeation constant
$Q(t)$	Cumulative flux (density) out of membrane
$Q_A(t)$	Cumulative flux out of membrane dependent on area

q_i, r_i	Constants of the multi-layer steady state solution which are independent of x and t
R	Universal gas constant
R_{H_2}	Specific gas constant for H_2
S, S_i	Solubility constant of material/layer
T	Absolute temperature
t	Time variable
$T_{n/m}(t)$	Temporal reduced eigenfunctions
u	Velocity of mass flux in porous material
$U(\rho)$, $V(\rho)$	Empirical functions for the calculation of the excess viscosity $\Delta\eta(\rho, T)$
V	Volume
v, v_i	Transient solution of membrane/layer
V_f	Volume of fluid/gas in porous material
w, w_i	Steady state solution of membrane/layer
x	Space variable
$X'_{i,m}(x)$	Derivative of spatial eigenfunctions for layer with respect to x
$X'_n(x)$	Derivative of reduced spatial eigenfunctions with respect to x
$X_{i,m}(x)$	Spatial reduced eigenfunctions for layer
x_i	Positions of the interfaces between layers in a multi-layer membrane
$X_n(x)$	Spatial reduced eigenfunctions for membrane
$Z(p, T)$	Compressibility factor

Introduction

In recent years, hydrogen has become more and more prominent as a potential solution for environment-friendly energy storage and transportation, though hydrogen storage is still the major challenge of this technology. Although several ways have been developed to store hydrogen, compressing hydrogen is still the most convenient and widely-used method. The main challenge here is the improvement of storage efficiency. While hydrogen density increases with increasing pressure, its compressibility factor increases as well, causing a rise of the required storage volume in contrast to an ideal gas. Therefore, storage efficiency can only be increased with raising the pressure inside the storage vessels, leading to storage concepts with pressures above 70 MPa [1–6].

The energy-to-weight-ratio of hydrogen storage vessels is further improved by replacing the metallic parts of vessels progressively with fiber-reinforced polymers. The main disadvantage of these materials is their inferior barrier properties compared to metals which usually show better characteristics concerning hydrogen permeation. The currently used polymers are often paired with metallic liners to improve the barrier properties. One major aim is to develop vessels with superior barrier properties without metallic materials to further reduce weight and costs of the vessels [1,3].

The development of such polymeric materials requires testing concepts to verify their suitability for hydrogen vessels. Suitable models have to be employed to get an optimum output of experimental data. During literature research, a lack of references with focus on mathematical and physical models for permeation of hydrogen at high pressure was found. On the one hand, models like time-lag and flow rate evaluation are established and easy to use. On the other hand, such simple models often require specific conditions to be valid or generate only limited information from measurement data. Therefore, this paper shall give an overview of models resulting from Fick's law and discuss their use in permeation experiments.

Three restrictions for the scope of this work are defined below:

1. The discussed models especially apply to experiments based on the differential pressure method. Such experiments are used to determine the permeation rate through a membrane by applying different partial pressures of the respective permeate at each face of the membrane. The different pressures cause a diffusion flow through the membrane which is either measured by measuring the progressively increasing pressure at the low-pressure face of the membrane or by detecting the permeating gas molecules. The differential pressure method is well-known resulting in several testing standards (e.g. Refs. [7,8]) and an abundant use in literature (e.g. Refs. [9–14]). Since it is possible to keep the pressures on either side of the membrane constant during the whole experiment and since such an experimental configuration very closely resembles the situation of a pressurized hydrogen vessel's wall, the differential pressure method is very well suited for the characterization of barrier materials and will be considered in the following.
2. In this work, the Laplace transformation will not be considered for solving any differential equation. Although the Laplace transformation facilitates the solution of the respective problems, the back transformation via an analytical approach is usually not feasible. Examples for such solutions are introduced by Crank [15] for single-layers. Laplace transformations are calculated for multi-layers by Carr et al. [16] or Rodrigo et al. [17] amongst other publications.
3. The aim of this work is to review models of Fickian diffusion for the evaluation of measurement results from the differential pressure method, focusing on hydrogen permeation through polymers with glass temperatures below the application temperature range. Therefore, the sorption-desorption processes will be described only with Henry sorption and no free volume models will be applied for diffusion processes. The work of Crank [18] as well as the reviews of Frisch et al. [19] and Kloppfer et al. [20] can

be recommended for information about free volume diffusion and further sorption models.

Single-layer permeation

Analytical solution

Derivation

Although the solution for Fick's 2. law

$$\frac{\partial C}{\partial t} = D \cdot \frac{\partial^2 C}{\partial x^2} \tag{2.1}$$

with the diffusion constant D and concentration C has already been derived in several works, especially prominent by Crank [15], a short sketch of the derivation is still given as an introduction into the latter derivations presented in this work for the sake of completeness. The initial and boundary conditions of the problem are restricted to the special case given by the differential pressure method

$$\begin{aligned} C(x,0) &= 0 \quad \text{for} \quad 0 < x < L \\ C(0,t) &= C_1 \quad \text{for} \quad 0 < t < \infty \\ C(L,t) &= C_2 \end{aligned} \tag{2.2}$$

where only measurements with "new" membranes (no initial concentration of the permeate inside the membranes) and constant conditions C_1 and C_2 at the faces of the membrane with thickness L are considered. This work is focused on 1D-problems, since the results are mostly sufficiently accurate. Possible edge effects can be neglected if the ratio between the membrane's radius and thickness is larger than 5 [15]. Furthermore, the expansion of these models to higher dimensions is straightforward.

Since the boundary conditions are inhomogeneous, the solution for $C(x,t)$ is separated into the steady-state $w(x)$ and the transient solution $v(x,t)$ according to

$$C(x,t) = w(x) + v(x,t). \tag{2.3}$$

With $\partial^2 w/\partial x^2 = 0$ and the boundary conditions in Eq. (2.2), it is straightforward to calculate the solution for the steady state

$$w(x) = (C_2 - C_1)\frac{x}{L} + C_1. \tag{2.4}$$

For the transient solution $v(x,t)$, separation of variables is used to solve Eq. (2.1)

$$v(x,t) = \tilde{T}(t) \cdot \tilde{X}(x) \tag{2.5}$$

which is divided by $D \cdot \tilde{T}(t) \cdot \tilde{X}(x)$ to receive

$$\frac{1}{D}\frac{1}{\tilde{T}(t)}\frac{\partial \tilde{T}}{\partial t} = \frac{1}{\tilde{X}(x)}\frac{\partial \tilde{X}^2}{\partial x^2} = -\lambda^2 \tag{2.6}$$

with $\lambda > 0$ for a non-trivial solution. Since the partial differential equation is separated into two ordinary differential equations, it is again straightforward to get the general solutions for $\tilde{T}(t)$ and $\tilde{X}(x)$

$$\begin{aligned} \tilde{T}(t) &= O \exp(-\lambda^2 D\, t) \\ \tilde{X}(x) &= M \sin(\lambda\, x) + K \cos(\lambda\, x) \end{aligned} \tag{2.7}$$

where O, H, and M are constants which are independent of x and t.

The boundary conditions for the transient solution are homogeneous ($v(0,t) = v(L,t) = 0$), since the steady state solution is already the result of the inhomogeneous boundary conditions in Eq. (2.2). Therefore, applying the homogeneous boundary conditions on $\tilde{X}(x)$ gives

$$\begin{aligned} H &= 0 \\ \lambda &= \frac{n\,\pi}{L} \text{ for } n \in \mathbb{N}. \end{aligned} \tag{2.8}$$

In general, O and M have different values for each eigenvalue λ_n, resulting in the eigenfunctions

$$\begin{aligned} \tilde{T}_n(t) &= O_n \exp\left(-n^2\,\pi^2\,\frac{D\,t}{L^2}\right) \\ \tilde{X}_n(x) &= M_n \sin\left(n\,\pi\,\frac{x}{L}\right). \end{aligned} \tag{2.9}$$

The eigenfunctions $\tilde{T}_n(t)$ and $\tilde{X}_n(x)$ form the general solution for the transient system $v(x,t)$ in accordance with

$$v(x,t) = \sum_{n=1}^{\infty} b_n \cdot \exp\left(-n^2\,\pi^2\,\frac{D\,t}{L^2}\right) \cdot \sin\left(n\,\pi\,\frac{x}{L}\right) \tag{2.10}$$

where $b_n = O_n \cdot M_n$. Since O_n and M_n, and therefore b_n, are arbitrary and independent of x and t, it has proven convenient to separate the coefficients of the infinite sum in Eq. (2.10) into the reduced eigenfunctions

$$\begin{aligned} T_n(t) &= \exp\left(-n^2\,\pi^2\,\frac{D\,t}{L^2}\right) \\ X_n(x) &= \sin\left(n\,\pi\,\frac{x}{L}\right) \end{aligned} \tag{2.11}$$

and the constants b_n. Inserting Eqs. (2.10) and (2.11) into Eq. (2.3) then gives

$$C(x,t) = w(x) + \sum_{n=1}^{\infty} b_n \cdot T_n(t) \cdot X_n(x) \tag{2.12}$$

for the concentration distribution $C(x,t)$ inside the membrane.

The explicit calculation of $v(x,t)$ from Eq. (2.12) along with the initial condition $C(x,0)$ at $t = 0$ (compare with Eq. (2.2)) yields to

$$v(x,0) = C(x,0) - w(x) = \sum_{n=1}^{\infty} b_n \cdot X_n(x). \tag{2.13}$$

Eq. (2.13) can be interpreted as a spectral analysis of $v(x,t)$, similar to the Fourier series, which describes how the system transforms from its initial state $C(x,0)$ to its steady state $w(x)$ over time. Contrary to the Fourier analysis, the eigenfunctions of the system are used instead of harmonic functions.

It has to be emphasized that the calculation of the coefficients b_n in the infinite sum in Eq. (2.13) can only be done analytically, if the eigenfunctions $X_n(x)$ are orthogonal to each other. The equations

$$\int_0^L \sin\left(n\,\pi\,\frac{x}{L}\right)\cdot\sin\left(m\,\pi\,\frac{x}{L}\right)dx = 0 \quad \text{for } n\neq m$$
$$\int_0^L \sin^2\left(n\,\pi\,\frac{x}{L}\right)dx = \frac{L}{2}\neq 0 \tag{2.14}$$

prove that the $X_n(x)$ eigenfunctions are orthogonal to each other. Hence, the infinite sum in Eq. (2.13) reduces to a single term when both of its sides are multiplied with $X_n(x)$ and integrated over the thickness of the membrane afterwards. The coefficients b_n are then calculated with

$$b_n = \frac{\int_0^L v(x,0)\,\sin\left(n\,\pi\,\frac{x}{L}\right)dx}{\int_0^L \sin^2\left(n\,\pi\,\frac{x}{L}\right)dx} \tag{2.15}$$

by using Eqs. (2.2) and (2.4) with Eq. (2.13).

The transient solution $v(x,t)$ is built by applying the result of Eq. (2.15) in Eq. (2.10). This result is used along with Eq. (2.4) in Eq. (2.12) which finally gives

$$C(x,t) = (C_2 - C_1)\frac{x}{L} + C_1 + \frac{2}{\pi}\cdot\sum_{n=1}^{\infty}\frac{(-1)^n\,C_2 - C_1}{n}\sin\left(n\,\pi\,\frac{x}{L}\right)e^{-n^2\,\pi^2\,\frac{D\,t}{L^2}}. \tag{2.16}$$

For the differential pressure method, not the concentration distribution inside the membrane $C(x,t)$ but the flux out of it $F(t)$ is of interest. Using Fick's 1. law

$$F(x,t) = -D\cdot\frac{\partial C(x,t)}{\partial x} \tag{2.17}$$

and then inserting the membrane thickness L for x results in

$$F(t) = D\cdot\frac{C_1 - C_2}{L} + \frac{2\,D}{L}\cdot\sum_{n=1}^{\infty}\left[(-1)^n\,C_1 - C_2\right]e^{-n^2\,\pi^2\,\frac{D\,t}{L^2}}. \tag{2.18}$$

for the flux density out of the membrane.

If $F(t)$ is integrated by t with the limits 0 and t and the identities $\sum_{n=1}^{\infty}1/n^2 = \pi^2/6$ and $\sum_{n=1}^{\infty}(-1)^n/n^2 = -\pi^2/12$ are used, the final solution for the cumulative flux density $Q(t)$ out of the membrane over time is

$$Q(t) = D\cdot\frac{C_1 - C_2}{L}\cdot t - \frac{(C_1 + 2\,C_2)\,L}{6} - \frac{2\,L}{\pi^2}\cdot\sum_{n=1}^{\infty}\frac{\left[(-1)^n\,C_1 - C_2\right]}{n^2}e^{-n^2\,\pi^2\,\frac{D\,t}{L^2}}\cdot \tag{2.19}$$

Non-dimensionalization of variables and functions

To reduce rounding errors or to ease fitting algorithms, it is often reasonable to use dimensionless variables in place of x and t for Eqs. (2.16), (2.18) and (2.19) [15]. A common form of non-dimensionalization is presented below (the hats denote normalized functions or dimensionless variables):

$$\widehat{C}_i = \frac{C_i}{C_1},\quad \widehat{x} = \frac{x}{L},\quad \tau = \frac{D\,t}{L^2}$$
$$C(x,t) = C_1\cdot\widehat{C}(\widehat{x},\tau)$$
$$F(t) = \frac{C_1\,D}{L}\cdot\widehat{F}(\tau)$$
$$Q(t) = C_1\,L\cdot\widehat{Q}(\tau) \tag{2.20}$$

Material characterization of single-layer membranes

Permeation experiments based on the differential pressure method are often performed to characterize the permeation properties of materials. Especially Eqs. (2.18) and (2.19) are employed for the evaluation of permeation properties of barrier materials. Very prominent examples for this are time-lag measurement, flow rate measurement or curve fitting.

Time-lag

The method of time-lag measurement was first developed by Daynes et al. [21] and later by Barrer et al. [22]. Even after 70 years, it is still a viable method for evaluating permeation measurements (e.g. Refs. [9,13,23–26]), where the cumulative flux $Q_A(t)$ is measured until the measurement approaches steady-state. A line $Q_A(t)_{steady}$ is fitted to the linear region of the obtained curve and intersected with the x- and y-axes (see Fig. 1). In doing so, $Q(t)_{steady}$ is calculated with $C_2 = 0$ and Eq. (2.19) in steady-state-form ($t\to\infty$, $\sum(\sim)\to 0$). Multiplying with the permeated area A then gives the area dependent cumulative flux

$$Q_A(t)_{steady} = A\cdot Q(t)_{steady} = \frac{A\,D\,C_1}{L}\cdot t - \frac{A\,C_1\,L}{6}. \tag{2.21}$$

Using the intersections I_1 and I_2 (Fig. 1) in Eq. (2.21) gives

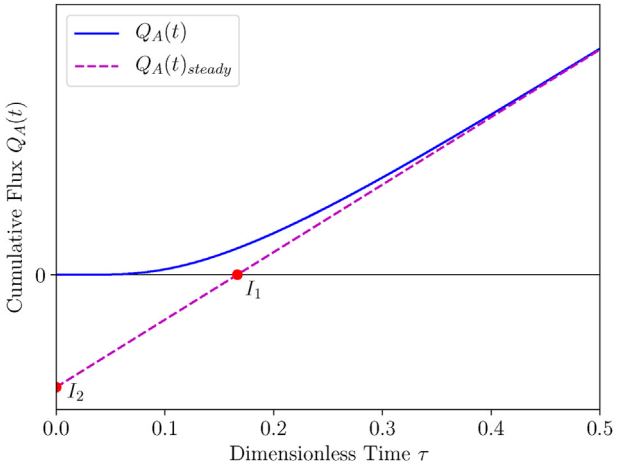

Fig. 1 – Example for $Q_A(t)$ over dimensionless time τ. Intersection I_1 between x-axis and the steady-state line gives the time-lag for the calculation of D while intersection I_2 on the y-axis is used for the calculation of C_1.

$$D = \frac{L^2}{6\, t_{l_1}}$$
$$C_1 = -\frac{6\, Q_A(0)_{steady}}{A\, L} \tag{2.22}$$

for the diffusion constant D and the concentration C_1.

If Henry sorption is valid, its relation can be used to derive the solubility constant S from the concentration C_1 and pressure p_1 at the respective membrane's face with

$$S = \frac{C_1}{p_1}. \tag{2.23}$$

Flow rate measurement

Multiplying Eq. (2.18) in steady-state form with A and using Eq. (2.23) gives

$$F_A = A\, D\, S\, \frac{p_1 - p_2}{L} \tag{2.24}$$

for the area dependent flow rate in steady-state. This resulting equation is often used to derive

$$Pe = D\, S \tag{2.25}$$

for the calculation of the permeation constant Pe from the diffusion constant D and the solubility constant S. Eq. (2.24) is often used in literature (e.g. Refs. [14,27–33]) and is the basic equation of the testing standards DIN 53380-2 [7] and ISO 15105-1 [8].

Curve fitting

Although, time-lag and flow rate measurements are well-established methods, there are several disadvantages. Foremost, both require the measurement system to approach steady-state. The first of the time dependent eigenfunctions in Eq. 2.11

$$T_1(t) = \exp\left(-\pi^2\, \frac{D\, t}{L^2}\right) \tag{2.26}$$

and the dimensionless time $\tau = D\, t/L^2$ can be used to get an estimate for the duration until steady-state. For example, after $\tau = 0.45$, $T_1(t)$ is still in the order of 10^{-2}. Hence, measurements can take a long time until steady-state is reached, depending on the diffusion constant D and the membrane thickness L. If the pressure is measured in a closed compartment for the cumulative flux $Q_A(t)$, the second assumption for time-lag measurement $C_2 = 0$ can become invalid after a time, which has to be specifically compensated [34,35].

The calculation of the error propagation from the time-lag measurements to the resulting material constants like D, S or Pe [26] is often of interest. Scheichl et al. [9] proposed to fit the measurements of cumulative flux $Q_A(t)$ to Eq. (2.19) with non-linear regression methods.

Fig. 2 shows an example for curve fitting of the cumulative flux $Q_A(t)$. The fitted testing data was prepared with Eq. (2.19) and superimposed with a 3%-sigma normal distributed noise. As Scheichl et al. [9] emphasized, linear regression methods for error estimation are possible in asymptotical approximation even for non-linear regression fits, if the minimum of the respective cost function features an elliptic shape (see Fig. 2b). This approach gives additional information about the measurement data, like errors of the material parameters or correlations between them. The correlation between diffusion constant D and face concentration C_1 amounts to -0.994 in case of the fit in Fig. 2. This value is reasonable if Eq. (2.25) is considered, where the diffusion constant D and solubility constant S should be indirectly proportional to each other (assuming Pe is constant).

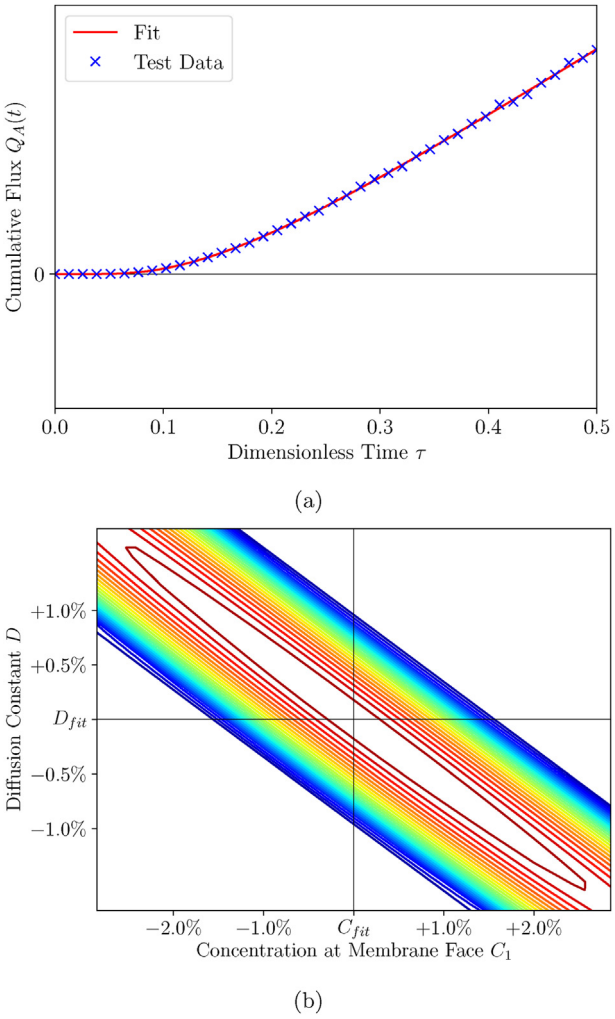

Fig. 2 – a) Fit of some test data generated with 3% random noise using Eq. (2.19) (multiplied with A), b) Contour plot of the cost function for the fit with varying parameters for D and C_1. Its minimum features an elliptic shape.

One major drawback of the curve fitting method is that computers are not able to process infinite sums like in Eqs. (2.16), (2.18) and (2.19). Fortunately, the magnitude of the elements of the sums decreases significantly with increasing n. Therefore, partial sums with a finite number of elements can be used for the equations. For short time durations t, artifacts which are caused by the missing remainder of the sum can be seen but they disappear with increasing t (see Fig. 3). In doing so the necessary number of elements is dependent on how small the dimensionless times of the fitted points become.

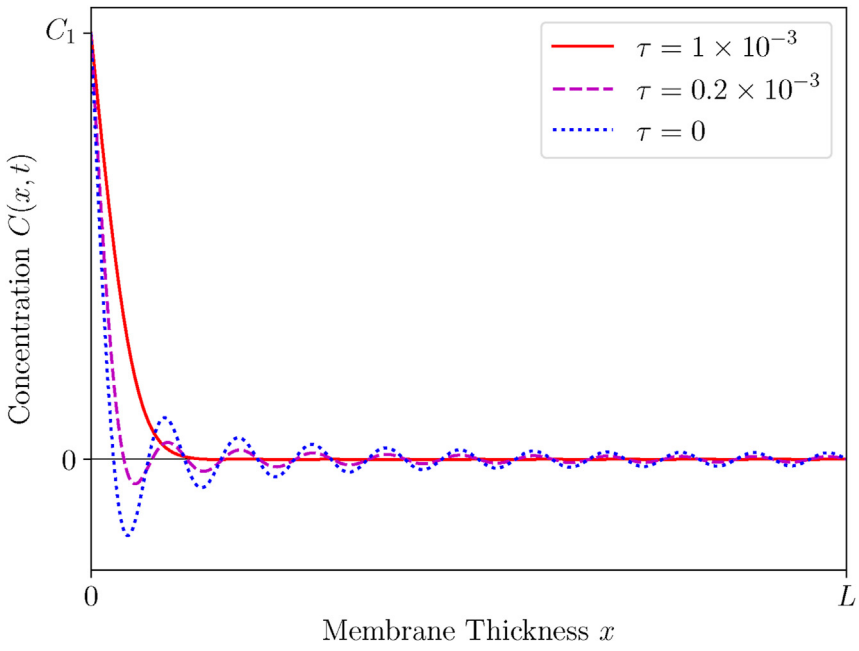

Fig. 3 – Example for artifacts in concentration C(x, t) ($C_2 = 0$) with $n_{max} = 20$ in Eq. (2.16). The artifacts disappear with increasing dimensionless time τ.

Concentration dependent diffusion in a single-layer

In the derivations above, it was assumed that the diffusion constant D was invariable. In some cases, the diffusion constant can be dependent on concentration, especially for larger gas molecules [9] or solvents [18]. Although, the diffusion constant seems to stay constant with hydrogen as permeate in polymers [19,20], no references were found in literature that this is still the case at high pressures. Scheichl et al. [9] presented a method to verify the presence of concentration dependency in diffusion by an objective significance test. Hence, some theory about concentration dependent diffusion is also included in this work.

Ash and Espenhahn derived several analytical time-lag methods [36–38]. But only the derivation by Frisch [39], which was also re-introduced by Crank [15] and Scheichl [9], is described in-depth in this work. Eq. (2.1) is transformed into an integral equation by spatially integrating it twice in the following way

$$\int_0^L \int_x^L \left[\frac{\partial C}{\partial t} - \frac{\partial}{\partial x'}\left(D(C)\cdot\frac{\partial C}{\partial x'}\right)\right] dx'\,dx = 0. \tag{2.27}$$

Integration of the second term in Eq. (2.27), together with Eq. (2.17) and inserting L for x, gives

$$\int_0^L \int_x^L \frac{\partial C}{\partial t}\,dx'\,dx + F(t)\cdot\int_0^L dx + \int_0^L D(C)\cdot\frac{\partial C}{\partial x}\,dx = 0. \tag{2.28}$$

Substitution of the integration variable to dC, solving Eq. (2.28) for $F(t)$, and integrating it by t give

$$Q(t) = \frac{1}{L}\left(\int_0^t dt' \int_{C_2}^{C_1} D(C)\,dC - \int_0^L \int_x^L C\,dx'\,dx\right). \tag{2.29}$$

The second integral is simplified by using the Theorem of Fubini-Tonelli [40], as one possible method for the calculation, to change the integration order

$$\begin{aligned}\int_0^L \int_x^L C\,dx'\,dx &= \int_0^L \int_0^L 1_{x\le x'} C\,dx'\,dx = \\ &= \int_0^L C \int_0^L 1_{x\le x'}\,dx\,dx' = \int_0^L C \int_0^{x'} dx\,dx' = \\ &= \int_0^L x'\,C\,dx'.\end{aligned} \tag{2.30}$$

The Theorem of Fubini-Tonelli applies if $C \ge 0$ in the range of the integral and if the integral exists and is finite. Both conditions are easily fulfilled by real-life concentrations in membranes. The insertion of Eq. (2.30) into Eq. (2.29) and the assumption of time-independent boundary conditions for the concentration finally yields to

$$Q(t) = \frac{1}{L}\left(t\int_{C_2}^{C_1} D(C)\,dC - \int_0^L x\,C\,dx\right). \tag{2.31}$$

If $D(C)$ is defined with an analytical function, the first integral can often be solved analytically. The second integral can only be solved by stating some assumptions (e.g. steady-state) [36–38]. Otherwise it has to be solved numerically.

Numerical models for single-layer diffusion

Basic numerical models and finite differences for the simulation of diffusion processes are beyond the scope of this work. For that, the book of Langtangen and Linge [41] is recommended as a starting point for the development of numerical algorithms.

Permeation through multiple layers

Analytical solution

Steady-state solution

Compared to single-layer permeation, models for permeation through multiple layers are considerably more complex. A good example for that are time-lag measurements. Ash et al. [42] found analytical expressions for time-lags of plane, cylindrical and spherical multi-layers, and their general solution was included in Crank [15]. The solution by Ash et al. is very complex in comparison to Eq. (2.22), and no easy way was found to apply Ash's solution to permeation measurements for material characterization.

A simple relation for plane membranes was published in the book of Crank [15]. It describes the total permeation constant of the multi-layered material based on the material constants of each layer material. The relation

$$\frac{L}{Pe} = \frac{L_1}{D_1\,S_1} + \frac{L_2}{D_2\,S_2} + \cdots + \frac{L_{n-1}}{D_{n-1}\,S_{n-1}} + \frac{L_n}{D_n\,S_n} \tag{3.1}$$

with L representing the total thickness of the membrane and Pe the resulting permeation constant was derived from Eqs. (2.24) and (2.25) and the condition of a constant flux through the multi-layer membrane in steady-state (see Fig. 4 for nomenclature).

Derivation of time-dependent solution

While Eq. (3.1) gives a good estimate for the resulting permeation constant of a membrane with multiple layers, verification of permeation experiments with such membranes may require models or simulations of the flux out of the membrane. Trefry et al. [44,45] and Hickson et al. [43,46–48] derived analytical solutions for diffusion within multiple layers. The derivation shown here bases on the work of Hickson et al. [47,48], which shows good readability and understandability. Since the solutions from Hickson et al. were specially derived for heat diffusion, the equations in this work were adapted for mass diffusion. Jump conditions between layers and general boundary conditions are not considered in this work to further increase comprehensibility.

The derivation for the multi-layer solution is comprehensive in Ref. [43], so just the crucial points of the derivation will be given in this work. Fick's laws (Eqs. (2.1) and (2.17)) are still valid in each layer with the respective material constants (see Fig. 4), but have to satisfy following boundary conditions (compare with Eq. (2.2)):

$$\begin{aligned} &C(x,0) = 0, \quad C(x_0,t) = C_1, \quad C(x_n,t) = C_2 \\ &\frac{C_i}{S_i} = \frac{C_{i+1}}{S_{i+1}} \\ &D_i \left.\frac{\partial C_i}{\partial x}\right|_{x_i} = D_{i+1} \left.\frac{\partial C_{i+1}}{\partial x}\right|_{x_i} \end{aligned} \tag{3.2}$$

The steady state solution is again the solution of $\partial^2 w/\partial x^2 = 0$:

$$w_i(x) = q_i\,(x - x_{i-1}) + r_i \tag{3.3}$$

where q_i and r_i are constants which are independent of x and t. The constants are determined with the boundary conditions in Eq. (3.2) and are calculated recursively with

$$\begin{aligned} q_i &= \frac{D_1}{D_i}\,q_1 \\ r_i &= \frac{S_i}{S_{i-1}}\,(r_{i-1} + q_{i-1}\,L_{i-1}) \end{aligned} \tag{3.4}$$

and

$$q_1 = \frac{\frac{C_2}{S_n} - \frac{C_1}{S_1}}{D_1 \sum_{i=1}^{n} \frac{L_i}{D_i\,S_i}} \tag{3.5}$$

$$r_1 = C_1.$$

The transient solution is again the solution of Eq. (2.1) using separation of variables, where $v_i(x,t) = X_i(x)\,T_i(t)$:

$$\frac{1}{T_i(t)}\frac{\partial T_i}{\partial t} = \frac{D_i}{X_i(x)}\frac{\partial X_i^2}{\partial x^2} = -\lambda^2. \tag{3.6}$$

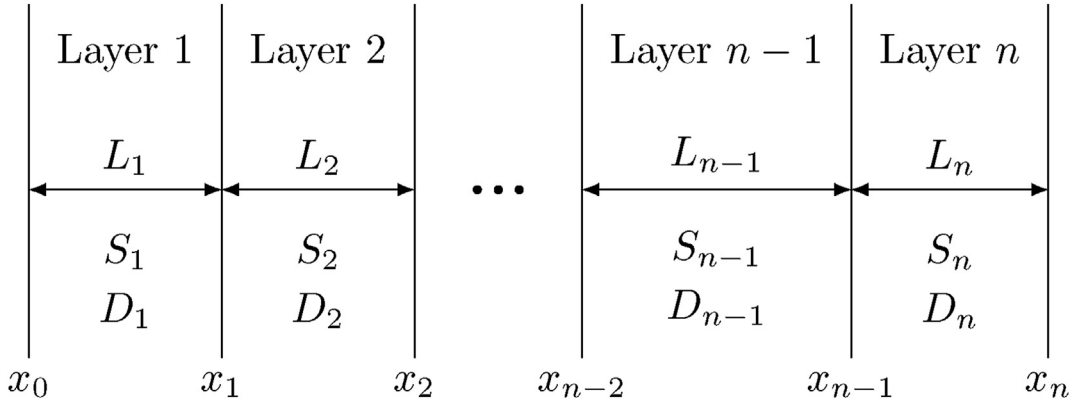

Fig. 4 – Multi-layer schematics showing the nomenclature of the derivation: D_i, S_i, L_i, and x_i are the respective diffusion constant, solubility constant, layer thickness, and the position of the layer interface in x [43]. (modified).

In case of multi-layers, the diffusion constants are part of the spatial solutions to validate the temporal solutions for all layers in the membrane. Solving the differential equations in Eq. (3.6) results in

$$T_m(t) = e^{-\lambda_m^2 t}$$
$$X_{i,m}(x) = J_{i,m}\sin\left(\frac{\lambda_m}{\sqrt{D_i}}(x - x_{i-1})\right) + K_{i,m}\cos\left(\frac{\lambda_m}{\sqrt{D_i}}(x - x_{i-1})\right) \tag{3.7}$$

where $J_{i,m}$ and $K_{i,m}$ are constants which are independent of x and t and λ_m are the eigenvalues. After the homogeneous boundary conditions $v(x_0,t) = v(x_n,t) = 0$ are applied, the constants are again calculated recursively with

$$J_{i+1,m}(x) = \frac{\sqrt{D_i}}{\sqrt{D_{i+1}}}\left[J_{i,m}\cos\left(\frac{\lambda_m L_i}{\sqrt{D_i}}\right) + K_{i,m}\sin\left(\frac{\lambda_m L_i}{\sqrt{D_i}}\right)\right]$$
$$K_{i+1,m}(x) = \frac{S_{i+1}}{S_i}\left[J_{i,m}\sin\left(\frac{\lambda_m L_i}{\sqrt{D_i}}\right) + K_{i,m}\cos\left(\frac{\lambda_m L_i}{\sqrt{D_i}}\right)\right] \tag{3.8}$$

and

$$J_{1,m} = 1$$
$$K_{1,m} = 0. \tag{3.9}$$

The eigenvalues λ_m are defined by the transcendental expression

$$J_{n,m}\sin\left(\frac{\lambda_m L_n}{\sqrt{D_i}}\right) + K_{n,m}\cos\left(\frac{\lambda_m L_n}{\sqrt{D_i}}\right) = 0 \tag{3.10}$$

which results from the homogeneous boundary condition $v(x_n, t) = 0$. This equation cannot be solved analytically, so its roots have to be found numerically.

Similarly to the derivation in Section 2.1.1, the constants b_m are derived from the expression for $v(x,0)$ (compare with Eq. (2.13)). Due to the orthogonality of the eigenfunctions $X_{i,m}(x)$ to each other (the mathematical proof can be found in the appendix of [43]), the constants b_m can be calculated with (compare with Eq. (2.15))

$$b_m = \frac{\sum_{i=1}^{n}\frac{1}{S_i}\int_{x_{i-1}}^{x_i} -w_i(x)\,X_{i,m}\,dx}{\sum_{i=1}^{n}\frac{1}{S_i}\int_{x_{i-1}}^{x_i} X_{i,m}^2\,dx} \tag{3.11}$$

where the initial condition in Eq. (3.2) is satisfied. The eigenvalues λ_m are the result of numerical calculations, so the integrals in Eq. (3.11) have to be calculated numerically, for example with Simpson's rule, too.

Analogous to Eq. (2.16), the time-dependent solution for the concentration distribution $C_i(x,t)$ in each layer of the membrane is then given by

$$C_i(x,t) = w_i(x) + \sum_{m=1}^{\infty} b_m\, e^{-\lambda_m^2 t}\, X_{i,m}(x) \tag{3.12}$$

where $w_i(x)$ and $X_{i,m}(x)$ are calculated with Eqs. (3.3) and (3.7), respectively.

Eq. (2.17) is again used to derive

$$F(t) = -D_n\left[q_n + \sum_{m=1}^{\infty} b_m\, e^{-\lambda_m^2 t}\, X_{n,m}'(L)\right] \tag{3.13}$$

with

$$X_{n,m}'(L) = \frac{\lambda_m}{\sqrt{D_n}}\left[J_{n,m}\cos\left(\frac{\lambda_m L_n}{\sqrt{D_i}}\right) - K_{n,m}\sin\left(\frac{\lambda_m L_n}{\sqrt{D_i}}\right)\right] \tag{3.14}$$

for the flux $F(t)$ out of the multi-layered membrane. The constant q_n is calculated with Eq. (3.4), with D_n as the diffusion constant of the last layer.

Integration of outgoing flux $F(t)$ by t gives the cumulative flux $Q(t)$ as in Section 2.1.1. In this case, no analytical identities for the infinite sum of the lower integration bound ($t = 0$) can be applied, since the constants λ_m and b_m are calculated numerically. In Section 2.2.3 the problem of artifacts when using finite sums for the calculation of the equation has already been mentioned. Just after a threshold time t_0, depending on the number of used sum elements M, the terms with higher order of the sums ($M+1, M+2,\ldots$) decrease below the machine accuracy.

Thus, the integration of $F(t)$ to calculate $Q(t)$ has to be split according to

$$Q(t) = \int_0^{t_0} F(t')\,dt' + \int_{t_0}^{t} F(t')\,dt'. \tag{3.15}$$

Because $F(t)$ is negligible at small times (see Fig. 5 for example), the first integral in Eq. (3.15) can be assumed as 0, but the accuracy can be increased by estimating the first integral with a linear approximation

$$\int_0^{t_0} F(t')\,dt' \approx \frac{F(t_0)\cdot t_0}{2} \tag{3.16}$$

resulting in the following equations for $Q(t)$

for $t \le t_0$:

$$Q(t) = \frac{F(t_0)\cdot t^2}{2\,t_0} \tag{3.17}$$

for $t > t_0$:

$$Q(t) = \frac{F(t_0)\cdot t_0}{2} - D_n\,q_n\,(t - t_0)$$
$$-D_n\sum_{m=1}^{M}\frac{b_m}{\lambda_m^2}\,X_{n,m}'(L)\left(e^{-\lambda_m^2 t_0} - e^{-\lambda_m^2 t}\right).$$

Since the formulas in Ref. [48] have been transcribed from heat diffusion to mass diffusion, the resulting equations had to be tested. Fig. 5 shows the comparison of the results of a simple 2D mass diffusion simulation implemented in the commercial software ABAQUS [49] and the analytical results from Eqs. (3.12) and (3.13).

The ABAQUS simulation is based on a rectangular 2D part with two material sections. The boundary conditions for concentration are applied at its left and right ends. The part was seeded with one row of 76 finite elements of type DC2D4 (quadrilateral elements for linear heat transfer) in a graded mesh in which the elements became progressively smaller toward high concentrations and toward the interface of the two layers.

The results from ABAQUS were extracted from the nodes of the elements in the simulation without further preprocessing. The numeric simulation corresponds well with the analytical calculation.

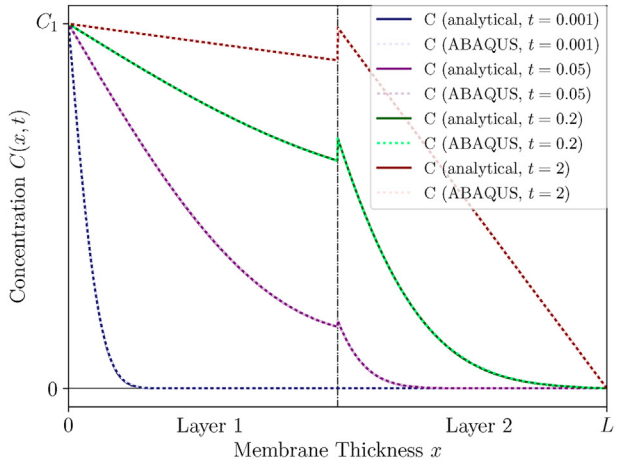

(a)

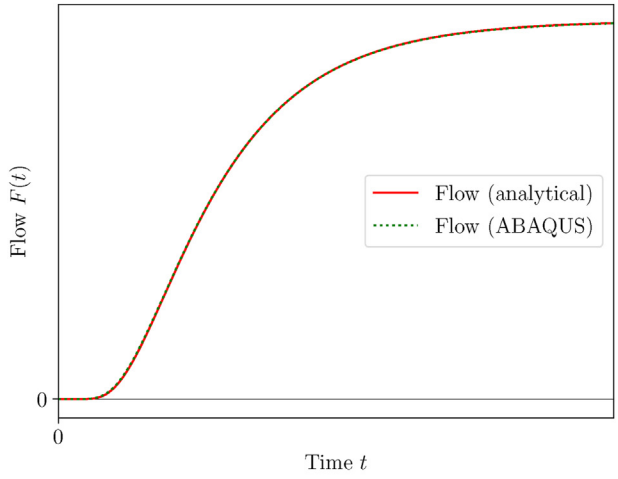

(b)

Fig. 5 – Comparison of ABAQUS simulation and analytical solution for a two-layer membrane: a) Concentration b) Flow (test parameters: $C(0,t) = 1$, $C(L,t) = 0$, $L_1 = 0.5$, $D_1 = 1$, $S_1 = 1$, $L_2 0.5$, $D_2 = 0.1$, $S_2 = 1.1$).

Non-dimensionalization for multi-layer-functions

At first sight, it is not obvious that the variables and functions derived in Section 3.1.2 can be non-dimensionalized like in Eq. (2.20), but comparison of the units shows that the unit of the eigenvalues λ_m is $s^{-1/2}$. With this fact in mind, the equation

$$\widehat{\lambda}_m = \frac{\lambda_m L}{\sqrt{D_1}} \tag{3.18}$$

can be derived from Eq. (3.7). Eq. (3.18) along with Eqs. (3.4), (3.5), (3.7) and (3.8) gives non-dimensionalization operations similar to Eq. (2.20):

$$\widehat{C}_i = \frac{C_i}{C_1}, \quad \widehat{x} = \frac{x}{L}, \quad \widehat{x}_i = \frac{x_i}{L}, \quad \tau = \frac{D_1\, t}{L^2}$$
$$\widehat{L}_i = \frac{L_i}{L}, \quad \widehat{D}_i = \frac{D_i}{D_1}, \quad \widehat{S}_i = \frac{S_i}{S_1}$$

$$C_i(x,t) = C_1 \cdot \widehat{C}_i(\widehat{x},\tau)$$
$$F(t) = \frac{C_1\, D_1}{L} \cdot \widehat{F}(\tau) \tag{3.19}$$
$$Q(t) = C_1\, L \cdot \widehat{Q}(\tau)$$

The permeation parameters of the first layer and the total thickness of the membrane L are used for the non-dimensionalization operations in Eq. (3.19).

Material characterization of membranes with multiple layers

Since the material constants D and S of a single-layer already strongly correlate to each other, the minimum of a cost function for a fit features flat slopes according to the correlation of the two material constants (see Fig. 2b) Therefore, noisy raw data strongly influences the fit parameters D and S while stable results are gained for Pe.

This effect increases for multiple layers because there is not only a strong correlation between the material constants of each layer but also among layers (see Eqs. (3.5) and (3.9)), which leads to larger uncertainties in the fitted material constants if measurements feature considerable noise. It is advisable to use the equations in Section 3.1.2 only with prior knowledge of the involved materials. One possibility is the simple verification or prediction of a measurement result for a multi-layered membrane if all layer materials are determined. Another one is to fit one layer or one material of a membrane while the rest of the layers or materials is known.

Numerical models for multiple layer diffusion

Hickson et al. [50] introduced several numerical models for diffusion processes in membranes with multiple layers. This work will be focused on what seems to be the most reasonable model for mass diffusion. In turn, the formulas are transcribed for mass diffusion, while jump conditions and general boundary conditions are ignored. Further, only the numerical determination of internal boundary conditions of the interfaces between the layers is introduced, since the numerical algorithms within the respective layers work in the same way as for single layers.

Fig. 6 depicts the concentrations at the grid points C_j around the interface at x_i. The intermediate points $C_{b\pm}$ are associated to the layers i and $i+1$ with different solubility constants S and diffusion constants D, respectively. The boundary conditions at interface x_i are similar to Eq. (3.2):

$$\frac{C_{b-}}{S_i} = \frac{C_{b+}}{S_{i+1}}$$
$$D_i \frac{\partial C_{b-}}{\partial x} = D_{i+1} \frac{\partial C_{b+}}{\partial x} \tag{3.20}$$

Hickson et al. [50] proposed to solve these boundary condition with 2nd order Taylor polynomials developed at $C_{b\pm}$. The resulting linear system with 6 equations and 6 unknowns was solved for $C_{b\pm}$. A shortcut by using the finite differences

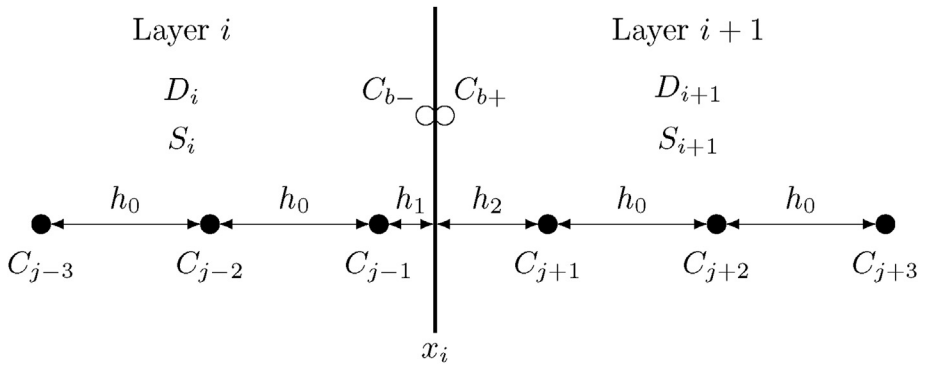

Fig. 6 – Schematic diagram of the grid points C_j (black dots) of the finite differences. i and j are the indices of the layers and the grid points, respectively. $C_{b\pm}$ denote the points on the interfaces between the layers but slightly to the left (negative) or right (positive) of the interface. h_0 is the spacing between the grid points. $h_{1,2}$ are the distances between the interface and the nearest points of the grid which can be different for each interface. This nomenclature was chosen to increase readability of the following equations [50]. (modified).

$$\frac{\partial C_{b-}}{\partial x} \approx \frac{C_{b-}\, h_0\, (h_0 + 2\, h_1) - C_{j-1}\, (h_0 + h_1)^2 + C_{j-2}\, h_1^2}{h_0\, h_1\, (h_0 + h_1)}$$
$$\frac{\partial C_{b+}}{\partial x} \approx \frac{-C_{b+}\, h_0\, (h_0 + 2\, h_2) + C_{j+1} (h_0 + h_2)^2 - C_{j+2}\, h_2^2}{h_0\, h_2\, (h_0 + h_2)} \tag{3.21}$$

is proposed here. The following linear system with only 2 equations and 2 unknowns results in the same analytical equations for the $C_{b\pm}$ as Hickson's approach because the finite differences are also developed at $C_{b\pm}$ with 2nd order Taylor polynomials. In order to reduce rounding errors, the spacing constants h_1, and h_2 have been substituted by

$$k_1 = \frac{h_1}{h_0}, \quad k_2 = \frac{h_2}{h_0} \tag{3.22}$$

while the numerators and denominators of the results for C_{b-} and C_{b+} are divided by the highest order of h_0. These operations finally give

$$\begin{aligned} C_{b-} = \frac{S_i}{\Lambda} \cdot \Big[& -D_i C_{j-2} \left(k_1^2 k_2^2 + k_1^2 k_2\right) \\ & + D_i C_{j-1} k_2 (k_1 + 1)^2 (k_2 + 1) \\ & + D_{i+1} C_{j+1} k_1 (k_1 + 1)(k_2 + 1)^2 \\ & - D_{i+1} C_{j+2} \left(k_1^2 k_2^2 + k_1 k_2^2\right) \Big] \end{aligned} \tag{3.23}$$

and

$$\begin{aligned} C_{b+} = \frac{S_{i+1}}{\Lambda} \cdot \Big[& -D_i C_{j-2} \left(k_1^2 k_2^2 + k_1^2 k_2\right) \\ & + D_i C_{j-1} k_2 (k_1 + 1)^2 (k_2 + 1) \\ & + D_{i+1} C_{j+1} k_1 (k_1 + 1)(k_2 + 1)^2 \\ & - D_{i+1} C_{j+2} \left(k_1^2 k_2^2 + k_1 k_2^2\right) \Big] \end{aligned} \tag{3.24}$$

with

$$\begin{aligned} \Lambda = {} & D_i\, S_i\, k_2\, (2\, k_1 + 1)\, (k_2 + 1) \\ & + D_{i+1}\, S_{i+1}\, k_1\, (k_1 + 1)\, (2\, k_2 + 1). \end{aligned} \tag{3.25}$$

These results for the internal boundary conditions can be used in the numerical simulation calculation of Eq. (2.1). Because of the varying grid spacing around the interfaces, the standard centered difference approximation for the second derivative cannot be used, but has to be adapted in the following way:

$$\frac{\partial^2 C_{j-1}}{\partial x^2} \approx 2 \cdot \frac{C_{b-}\, h_0 - C_{j-1}\, (h_0 + h_1) + C_{j-2}\, h_1}{h_0\, h_1\, (h_0 + h_1)}$$
$$\frac{\partial^2 C_{j+1}}{\partial x^2} \approx 2 \cdot \frac{C_{b+}\, h_0 - C_{j+1}\, (h_0 + h_2) + C_{j+2}\, h_2}{h_0\, h_2\, (h_0 + h_2)}. \tag{3.26}$$

Furthermore, the transcription from heat diffusion to mass diffusion was tested. Fig. 7 shows the comparison of the analytical solution and the numerical calculation (see also Fig. 5a). The Crank-Nicholson approach [15,41] was used along with the results introduced in this section for the numerical diffusion simulation. Very small numbers were used for the time step Δt and the grid spacing h_0 to let the results of the numerical simulation converge to the analytical solution.

Influence of porous plates on permeation measurements

Porous plates are considered as a part of the differential pressure method in this work. Other works (e.g. Refs. [51,52]) are recommended for in-depth information about porous materials.

Polymer membranes and thin barrier films are often not strong enough to withstand the forces of the pressure differences in the differential pressure method. Sintered metallic porous membranes are often introduced to mechanically reinforce the organic membranes [12,53], preferably without influencing the measurements of the polymer membranes too strongly. Hence, such porous materials have to feature comparably high permeation rates and high mechanical stability at the same time. Technical datasheets of such porous materials unveil that a high mechanical stability is mostly

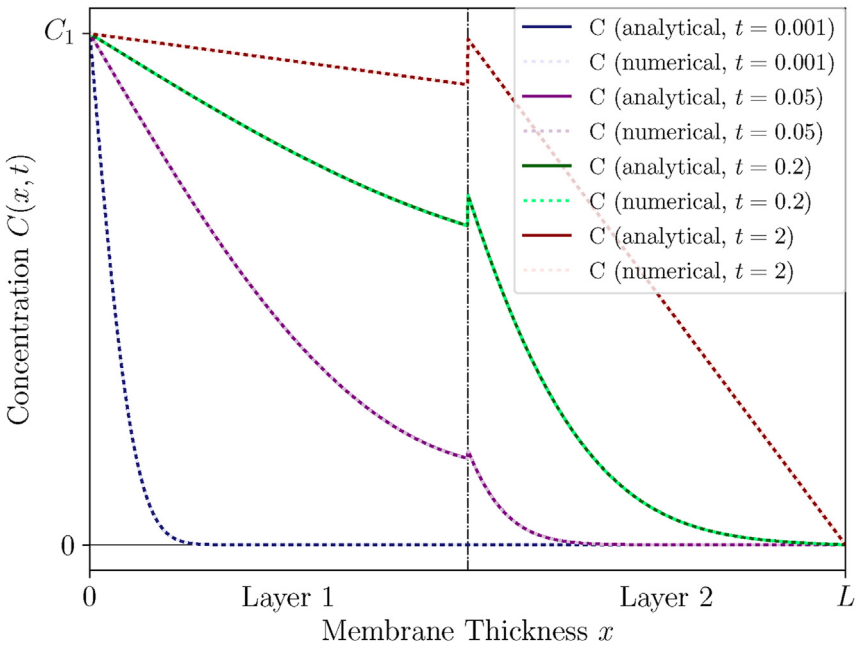

Fig. 7 – Comparison of the numerical calculation based on Hickson et al. [50] and the analytical solution for the concentration distribution in a two-layer membrane (test parameters: $(\Delta t = 5.10^{-7}$, $h_0 = L/10^3$, $C(0,t) = 1$, $C(L,t) = 0$, $L_1 = 0.5$, $D_1 = 1$, $S_1 = 1$, $L_2 = 0.5$, $D_2 = 0.1$, $S_2 = 1.1$).

achieved at the expense of low permeability and vice versa (e.g. Ref. [54][1]).

Contradictionally, experimental work by Fujiwara et al. [12] denies a significant influence of porous plates on the differential pressure method. Nevertheless, it is recommended to quantify this influence in a theoretical estimate to rule out systematic errors in the measurements.

Hydrogen gas properties

The permeation of gases through porous materials is also strongly dependent on the gas density ρ and the gas viscosity μ. It is sufficient under standard conditions to use the ideal gas equation

$$p\,V = n\,R\,T = m\,R_{H_2}\,T \tag{4.1}$$

with pressure p, gas volume V, the amount of substance n, the universal gas constant R and the absolute temperature T, or mass m and the specific gas constant for hydrogen R_{H_2}, to derive a relationship between pressure and gas density. Although this relation seems rather simple, its results for high pressures, as in hydrogen vessels, are not satisfactory. To counter this, the compressiblity factor Z is added to the ideal gas equation giving

$$p\,V = n\,R\,T\,Z(p,T) = m\,R_{H_2}\,T\,Z(p,T). \tag{4.2}$$

The compressibility factor Z is dependent on temperature T and pressure p. Younglove [56] and Lemmon et al. [57] developed relationships between density and pressure of hydrogen which are valid over a range of temperature and pressure. Later these relationships were revised by Leachman et al. [58] and Lemmon et al. [59] to expand the ranges of validity for temperature and pressure. It seems that especially the relationship for the compressibility Z

$$Z(p,T) = 1 + \sum_{i=1}^{9} a_i \left(\frac{100\ \mathrm{K}}{T}\right)^{b_i} \left(\frac{p}{1\ \mathrm{MPa}}\right)^{c_i} \tag{4.3}$$

which was found by Lemmon et al. [59] is important for hydrogen applications and the differential pressure method.

The values for the constants a_i, b_i, and c_i are shown in Table 1. Lemon et al. estimated the uncertainty of this equation to be 0.15 % for temperatures in a range between 150 K and 1000 K and for pressures up to 200 MPa. In Fig. 8, the comparison of the ideal gas equation and Eq. (4.2) used with Eq. (4.3) is shown.

Also, the viscosity of hydrogen is strongly dependent on temperature and pressure. Yusibani et al. [60] found an empirical correlation based on the Chapman-Enskog solution [61] for the viscosity at the limit $\rho = 0$

$$\eta_0(T) = \frac{5}{16}\,\frac{\sqrt{\pi\,m\,k_B\,T}}{\pi\,\sigma^2\,\Omega_\eta(T)} \tag{4.4}$$

and the excess viscosity theory

$$\eta(T,\rho) = \eta_0(T) + \Delta\eta(T,\rho) \tag{4.5}$$

which extends the work of Diller and Dwain [62]. The collision integral $\Omega_\eta(T)$ in Eq. (4.4) is expressed by

$$\Omega_\eta(T) = \exp\left[\sum_{i=0}^{4} o_i \ln\left(\frac{T}{\varepsilon/k_B}\right)^i\right] \tag{4.6}$$

which was developed by Assael et al. [63]. Yusibani et al. [60] proposed the values for the Lennard-Jones parameters

[1] Zhu et al. [55] give a comprehensive review about additional suppliers for sintered metallic porous plates.

Table 1 – Constants a_i, b_i, and c_i which are used in Eq. (4.3) [59].

i	a_i	b_i	c_i
1	0.05888460	1.325	1.0
2	−0.06136111	1.87	1.0
3	−0.002650473	2.5	2.0
4	0.002731125	2.8	2.0
5	0.001802374	2.938	2.42
6	−0.001150707	3.14	2.63
7	9.588528e-5	3.37	3.0
8	−1.10904e-7	3.75	4.0
9	1.264403e-10	4.0	5.0

$\sigma = 0.296$ nm and $\varepsilon/k_B = 35$ K for hydrogen to calculate Eqs. (4.4) and (4.6). k_B is the Boltzmann constant and T the absolute temperature.

The excess viscosity $\Delta\eta(T,\rho)$ is calculated with the expression

$$\Delta\eta(T,\rho) = U(\rho)\,\exp\left[\frac{V(\rho)}{T}\right] \tag{4.7}$$

with

$$U(\rho) = \rho\cdot\exp\left[u_0 + u_1\,\rho^{\frac{3}{2}} - u_2\,\exp(u_3\,\rho)\right] \tag{4.8}$$

and

$$V(\rho) = \left\{s_0 + s_1\left[\left(\frac{\rho}{0.07}\right)^6 + \left(\frac{\rho}{0.07}\right)^{\frac{3}{2}}\right] + s_2\,\exp\left[s_3\left(\frac{\rho}{0.07}\right)^3\right]\right\}[\mathrm{K}]. \tag{4.9}$$

The constants o_i, u_i, and s_i for the calculation of Eqs. (4.6), (4.8) and (4.9) are shown in Table 2. The hydrogen gas density ρ is calculated with Eq. (4.3).

The equations for hydrogen viscosity by Yusibani et al. [60] are valid in a pressure range from 0.1 MPa to 220 MPa and in a temperature range from 100 K to 990 K. The deviation between this correlation and the investigated experimental data was between 2 % and 4 %.

Steady state estimate for the influence of porous membranes on the differential pressure measurements

Time-dependent consideration of gas flux through porous materials by means of computational fluid dynamics (e.g. Refs. [64–68]) and experimental determination of the pressure loss in porous plates (e.g. Refs. [69–73]) are beyond the scope of this work, but an estimation of the influence of porous plates on measurement results of the differential pressure method is of interest. A rough calculation is proposed which mainly bases on the considerations of Zhong et al. [69].

The gas velocity u through a porous plate is calculated with

$$u = \frac{F_A}{\rho\,\varphi\,A} \tag{4.10}$$

where ρ is the gas density, φ the porosity of the material, and A is the cross-sectional area of the flux. Since the flux F_A through the dense membrane and the porous plate is considered as continuous, it can be calculated with Eq. (2.24) giving

$$u = \frac{D\,S_m}{\rho\,\varphi}\,\frac{\Delta p_{dense}}{L_{dense}}. \tag{4.11}$$

The solubility constant S_m is adapted using Eq. (4.2) to give a mass flux instead of a concentration or volume flux.

The Forchheimer equation [74].

$$\frac{\eta}{K_D}\,u + \frac{\rho}{K_F}\,u^2 = -\frac{\partial p}{\partial x} \approx \frac{\Delta p_{porous}}{L_{porous}} \tag{4.12}$$

where K_D is the Darcy permeability and K_F is the Forchheimer constant can be derived from the Navier-Stokes-Equations for porous plates [75,76]. Eq. (4.12) is used along with Eq. (4.11) to calculate the pressure loss Δp_{porous} over the thickness of the

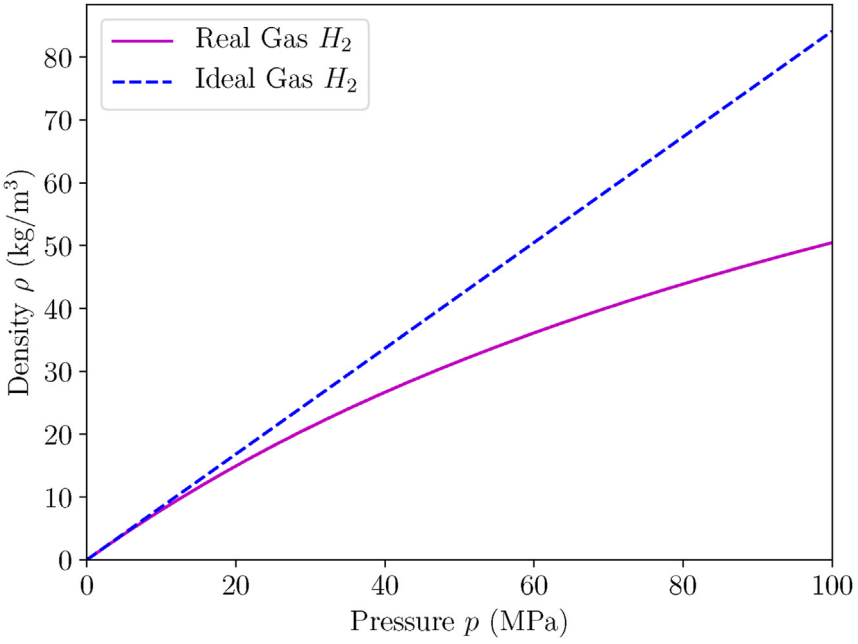

Fig. 8 – Comparison of results of the ideal gas equation and from Eq. 4.3 for hydrogen.

Table 2 – Constants o_i, u_i, and s_i which are used in Eqs. (4.6), (4.8) and (4.9) [60].

i	o_i	u_i	s_i
0	0.354125	5.73	10.0
1	−0.427581	65.0	8.0
2	0.149251	6.0e-6	18.0
3	−0.037174	135.0	59.0
4	0.003176	–	–

Table 3 – Test parameters for Algorithm 1.

Parameters	Values	units
Diffusion constant D [77]	7.305×10^{-11}	$\frac{m^2}{s}$
Solubility constant S_m [77]	1.067×10^{-7}	$\frac{kg}{Pa \cdot m^3}$
Thickness L_{dense}	2×10^{-3}	m
Darcy Constant K_D [54]	2×10^{-13}	m^2
Forchheimer Constant K_F [54]	1×10^{-8}	m
Thickness L_{porous}	4×10^{-3}	m
High pressure p_0	1×10^{8}	Pa
Low pressure p_2	1×10^{5}	Pa

porous plate L_{porous}. Equating the expressions for the flux through the dense membrane and the flux through the porous plate gives the estimation

$$Pe_{porous} = D\, S_m \frac{L_{porous}}{L_{dense}} \frac{\Delta p_{dense}}{\Delta p_{porous}} \tag{4.13}$$

for the permeation constant for the porous plate Pe_{porous}

Algorithm 1 applied to the test parameters in Table 3 gives a pressure loss $\Delta p = 3.5$ Pa for the porous plate. This results in a 5×10^7 times larger permeation constant of the porous plate compared to the HDPE-membrane which confirms the results in Ref. [12] along with Eq. (3.1). If the order of the dense membrane and the porous plate is reversed with the porous plate at the high pressure side, the pressure loss is even lower. Since the gas density ρ is considerably higher at the high pressure side, the gas flow through the porous plate is even slower for the same mass flow through the membranes.

Algorithm 1: Optimization Algorithm for interface pressure p_1 and Pe_{porous}

$p_0 = \text{constant}_{boundary}$;
$p_2 = \text{constant}_{boundary}$;
$p_1 = \text{constant}_{start\ value}$;
$p_{diff} = \text{constant} > \epsilon$;
while $p_{diff} > \epsilon$ **do**
  $p_{mean} = 0.5 \cdot (p_1 + p_2)$;
  Calculate η and ρ from equations in Section 4.1 using p_{mean};
  Calculate u with Eq. (4.11);
  ;
  Use u in Eq. (4.12) and solve for p_1;
  $p_{diff} = \|p_{1new} - p_{1old}\|$;
Calculate Pe_{porous} with Eq. (4.13);
Result: Optimized results for p_1 and Pe_{porous}

Summary and outlook

The differential pressure method is a common testing setup for the measurement of gas permeation through a membrane. Especially, hydrogen as potential new energy source has become one of the main topics of recent permeation studies. In this review the most common models for hydrogen permeation through polymer membranes were analyzed and evaluated. Analytical and numerical models were discussed for single and multi-layer membranes. Furthermore, the models for the most important gas properties of hydrogen were investigated. These models were also used to estimate the influence of porous plates, which are often used in differential pressure setups, on measurement results. The assumptions and applications for each model were discussed comprehensively to be readily useable for the evaluation of hydrogen permeation data from the differential pressure method.

The advantages of curve fitting methods were emphasized over time-lag and flow rate measurements. Since steady-state is unnecessary, measurement durations can be significantly shortened. Additional information is obtained like error propagation to material parameters or the correlation between fitting parameters.

Only a single literature reference was found which concerns the influence of porous plates in a differential pressure setup [12]. Hence, it seemed necessary to provide a simple way for estimating the influence of porous plates. The results of the estimation, along with the experimental results in the reference, confirm that porous plates do not influence the measurements of barrier materials significantly.

The intention to write this paper was to provide a base for the future development of permeation models, especially for high pressure storage applications of hydrogen. The new models are needed to predict permeation results with higher accuracy, reduce the durations of experimental work, or predict permeation properties of polymers according to their structure and composition. Objective significance tests which are easily obtained from the approved models in this paper along with curve fitting algorithms [9] will facilitate the evaluation and validation of the new models.

Additional to the differential pressure method, further potential applications for the reviewed models arise in case of decompression failures of high pressure storage vessels for hydrogen, like collapse of liners from vessel walls (e.g. Refs. [78–82]) or the damage in polymers due to rapid gas decompression (e.g. Refs. [83–89]), since the models also describe the concentration distribution inside the permeated materials or laminates. Additional research is necessary to apply the models on such problems because boundary conditions and system geometries of the models have to be adjusted accordingly. Further, it has to be investigated if jump conditions in the multilayered models are required to describe liner collapse specifically.

Declaration of competing interest

The authors declare that they have no known competing financial interests or personal relationships that could have appeared to influence the work reported in this paper.

Acknowledgements

The research work was performed within the COMET-modul "Polymers4Hydrogen" (project-no.: 872165) at the Polymer Competence Center Leoben GmbH (PCCL, Austria) within the framework of the COMET-program of the Federal Ministry for Transport, Innovation and Technology and the Federal Ministry for Digital and Economic Affairs. The COMET-modul is funded by the Austrian Government and the State Government of Styria.

REFERENCES

[1] Sasaki K, Li H-W, Hayashi A, Yamabe J, Ogura T, Lyth SM, editors. Hydrogen energy engineering: a Japanese perspective, green energy and Technology. Tokyo and s.l., Springer Japan; 2016. http://dx.doi.org/10.1007/978-4-431-56042-5.

[2] Fayaz H, Saidur R, Razali N, Anuar FS, Saleman AR, Islam MR. An overview of hydrogen as a vehicle fuel. Renew Sustain Energy Rev 2012;16(8):5511–28. http://dx.doi.org/10.1016/j.rser.2012.06.012.

[3] Mori D, Hirose K. Recent challenges of hydrogen storage technologies for fuel cell vehicles. Int J Hydrogen Energy 2009;34(10):4569–74. http://dx.doi.org/10.1016/j.ijhydene.2008.07.115.

[4] Jain IP. Hydrogen the fuel for 21st century. Int J Hydrogen Energy 2009;34(17):7368–78. http://dx.doi.org/10.1016/j.ijhydene.2009.05.093.

[5] Schlapbach L, Züttel A. Hydrogen-storage materials for mobile applications. Nature 2001;414(6861):353–8. http://dx.doi.org/10.1038/35104634.

[6] Sgobbi A, Nijs W, de Miglio R, Chiodi A, Gargiulo M, Thiel C. How far away is hydrogen? Its role in the medium and long-term decarbonisation of the European energy system. Int J Hydrogen Energy 2016;41(1):19–35. http://dx.doi.org/10.1016/j.ijhydene.2015.09.004.

[7] Din 53380-2: prüfung von Kunststoffen – bestimmung der Gasdurchlässigkeit – teil 2: manometrisches Verfahren zur Messung an Kunststoff-Folien. November 2006.

[8] ISO 15105-1: plastics — film and sheeting - determination of gas-transmission rate — Part 1: differential-pressure methods. 2007-10-15.

[9] Scheichl R, Klopffer MH, Benjelloun-Dabaghi Z, Flaconneche B. Permeation of gases in polymers: parameter identification and nonlinear regression analysis. J Membr Sci 2005;254(1–2):275–93. http://dx.doi.org/10.1016/j.memsci.2005.01.019.

[10] Hunt PA, Ashworth CR, Matthews RP. Hydrogen bonding in ionic liquids. Chem Soc Rev 2015;44(5):1257–88. http://dx.doi.org/10.1039/C4CS00278D.

[11] Naito Y, Kamiya Y, Terada K, Mizoguchi K, Wang J-S. Pressure dependence of gas permeability in a rubbery polymer. J Appl Polym Sci 1996;61(6):945–50. http://dx.doi.org/10.1002/(SICI)1097-4628(19960808)61:6<945::AID-APP8>3.0.CO;2-H.

[12] H. Fujiwara, H. Ono, K. Onoue, S. Nishimura, High-pressure gaseous hydrogen permeation test method -property of polymeric materials for high-pressure hydrogen devices (1)-, Int J Hydrogen Energy:10.1016/j.ijhydene.2020.07.215.

[13] Fraga SC, Monteleone M, Lanč M, Esposito E, Fuoco A, Giorno L, Pilnáček K, Friess K, Carta M, McKeown NB, Izák P, Petrusová Z, Crespo JG, Brazinha C, Jansen JC. A novel time lag method for the analysis of mixed gas diffusion in polymeric membranes by on-line mass spectrometry: method development and validation. J Membr Sci 2018;561:39–58. http://dx.doi.org/10.1016/j.memsci.2018.04.029.

[14] Flaconneche B, Martin J, Klopffer MH. Permeability, diffusion and solubility of gases in polyethylene, polyamide 11 and poly (vinylidene fluoride). Oil Gas Sci Technol 2001;56(3):261–78. http://dx.doi.org/10.2516/ogst:2001023.

[15] Crank J. The mathematics of diffusion. 2nd ed. Oxford: Clarendon Press; 1976.

[16] Carr EJ, March NG. Semi-analytical solution of multilayer diffusion problems with time-varying boundary conditions and general interface conditions. Appl Math Comput 2018;333:286–303. http://dx.doi.org/10.1016/j.amc.2018.03.095. URL, http://arxiv.org/pdf/1705.09925v3.

[17] Rodrigo MR, Worthy AL. Solution of multilayer diffusion problems via the Laplace transform. J Math Anal Appl 2016;444(1):475–502. http://dx.doi.org/10.1016/j.jmaa.2016.06.042.

[18] Crank J, Park GS. Diffusion in polymers. 3rd ed. London: Acad. Pr; 1977.

[19] Frisch HL. Sorption and transport in glassy polymers-a review. Polym Eng Sci 1980;20(1):2–13. http://dx.doi.org/10.1002/pen.760200103.

[20] Klopffer MH, Flaconneche B. Transport properties of gases in polymers: bibliographic review. Oil Gas Sci Technol 2001;56(3):223–44. http://dx.doi.org/10.2516/ogst:2001021.

[21] Daynes HA. The process of diffusion through a rubber membrane. Proc R Soc Lond - Ser A Contain Pap a Math Phys Character 1920;97(685):286–307. http://dx.doi.org/10.1098/rspa.1920.0034.

[22] Barrer RM, Rideal EK. Permeation, diffusion and solution of gases in organic polymers. Trans Faraday Soc 1939;35:628. http://dx.doi.org/10.1039/TF9393500628.

[23] Chapelle D, Feng LP, Nardin P, Rauch JY. Assessment of the Gas Permeation Through Thin Coated Polymeric Membranes; Improvement of the Gas Barrier Ability for Hydrogen Storage, Defect and Diffusion Forum. 2012. p. 393. http://dx.doi.org/10.4028/www.scientific.net/DDF.323-325.393.

[24] B. Craster, T. G. J. Jones, Permeation of a range of species through polymer layers under varying conditions of temperature and pressure: in situ measurement methods, Polymers 11 (6). doi:10.3390/polym11061056.

[25] Monson L, Moon SI, Extrand CW. Permeation resistance of poly(ether ether ketone) to hydrogen, nitrogen, and oxygen gases. J Appl Polym Sci 2013;127(3):1637–42. http://dx.doi.org/10.1002/app.37517.

[26] Wu H, Kruczek B, Thibault J. Impact of measuring devices and data analysis on the determination of gas membrane properties. J Memb Sci Res 2018;4(1):4–14. http://dx.doi.org/10.22079/JMSR.2017.63433.1136.

[27] Firpo G, Angeli E, Guida P, Lo Savio R, Repetto L, Valbusa U. Gas permeation through rubbery polymer nano-corrugated membranes. Sci Rep 2018;8(1):6345. http://dx.doi.org/10.1038/s41598-018-24551-4.

[28] George SC, Thomas S. Transport phenomena through polymeric systems. Prog Polym Sci 2001;26(6):985–1017. http://dx.doi.org/10.1016/S0079-6700(00)00036-8.
[29] Hermkes R, Colmer H, Ophoff H. Modern PE pipe enables the transport of hydrogen. In: Proc 19th Plast Pipes Conf PPXIX, Sept; 2018. p. 24–6.
[30] Humpenöder J. Gas permeation of fibre reinforced plastics. Cryogenics 1998;38(1):143–7. http://dx.doi.org/10.1016/S0011-2275(97)00125-2.
[31] Klopffer M-H, Berne P, Espuche É. Development of innovating materials for distributing mixtures of hydrogen and natural gas. Study of the barrier properties and durability of polymer pipes. Oil Gas Sci Technol 2015;70(2):305–15. http://dx.doi.org/10.2516/ogst/2014008.
[32] Lagaron JM, Catalá R, Gavara R. Structural characteristics defining high barrier properties in polymeric materials. Mater Sci Technol 2013;20(1):1–7. http://dx.doi.org/10.1179/026708304225010442.
[33] Mukaddam M, Litwiller E, Pinnau I. Pressure-dependent pure- and mixed-gas permeation properties of Nafion\circledR. J Membr Sci 2016;513:140–5. http://dx.doi.org/10.1016/j.memsci.2016.04.042.
[34] Paul DR, DiBenedetto AT. Diffusion in amorphous polymers. J Polym Sci Part C: Polymer Symposia 1965;10(1):17–44. http://dx.doi.org/10.1002/polc.5070100105.
[35] Jenkins RCL, Nelson PM, Spirer L. Calculation of the transient diffusion of a gas through a solid membrane into a finite outflow volume. Trans Faraday Soc 1970;66:1391. http://dx.doi.org/10.1039/TF9706601391.
[36] Ash R, Espenhahn SE. Transport through a slab membrane governed by a concentration-dependent diffusion coefficient. Part I. The four time-lags: some general considerations. J Membr Sci 1999;154(1):105–19. http://dx.doi.org/10.1016/S0376-7388(98)00286-5.
[37] Ash R, Espenhahn SE. Transport through a slab membrane governed by a concentration-dependent diffusion coefficient III. J Membr Sci 2000;180(1):133–46. http://dx.doi.org/10.1016/S0376-7388(00)00530-5.
[38] Ash R, Espenhahn SE, Whiting DE. Transport through a slab membrane governed by a concentration-dependent diffusion coefficient II. J Membr Sci 2000;166(2):281–301. http://dx.doi.org/10.1016/S0376-7388(99)00272-0.
[39] Frisch HL. The time lag in diffusion. Br J Appl Phys 1957;61(1):93–5. http://dx.doi.org/10.1021/j150547a018.
[40] Fubini G. Sugli integrali multipli, Accademia dei Lincei. Rendiconti, V. Serie 1907;16(1):608–14.
[41] Langtangen HP, Linge S. Finite difference computing with PDEs, vol. 16. Cham: Springer International Publishing; 2017. http://dx.doi.org/10.1007/978-3-319-55456-3.
[42] Ash R, Barrer RM, Palmer DG. Diffusion in multiple laminates. Br J Appl Phys 1965;16(6):873–84. http://dx.doi.org/10.1088/0508-3443/16/6/314.
[43] Hickson RI, Barry SI, Mercer GN. Critical times in multilayer diffusion. Part 1: exact solutions. Int J Heat Mass Tran 2009;52(25–26):5776–83. http://dx.doi.org/10.1016/j.ijheatmasstransfer.2009.08.013.
[44] Trefry MG. Analytical solutions for partitioned diffusion in laminates: II. Harmonic forcing conditions. Transport Porous Media 1999;37(2):183–212. http://dx.doi.org/10.1023/A:1006562700905.
[45] Trefry MG, Whyte DS. Analytical solutions for partitioned diffusion in laminates: I. Initial value problem with steady cauchy conditions. Transport Porous Media 1999;37(1):93–128. http://dx.doi.org/10.1023/A:1006566125433.
[46] Hickson R, Barry S, Mercer G. Exact and numerical solutions for effective diffusivity and time lag through multiple layers. ANZIAM J 2008;50:682. http://dx.doi.org/10.21914/anziamj.v50i0.1386.
[47] Hickson RI, Barry SI, Sidhu HS. Critical times in one- and two-layered diffusion. Australas J Eng Educ 2009;15(2):77–84. http://dx.doi.org/10.1080/22054952.2009.11464024.
[48] Hickson RI, Barry SI, Mercer GN. Critical times in multilayer diffusion. Part 2: approximate solutions. Int J Heat Mass Tran 2009;52(25–26):5784–91. http://dx.doi.org/10.1016/j.ijheatmasstransfer.2009.08.012.
[49] Dassault Systems Simulia Corp. ABAQUS 2019 [Software]. 2018. https://www.3ds.com/de/produkte-und-services/simulia/produkte/abaqus/.
[50] Hickson RI, Barry SI, Mercer GN, Sidhu HS. Finite difference schemes for multilayer diffusion. Math Comput Model 2011;54(1–2):210–20. http://dx.doi.org/10.1016/j.mcm.2011.02.003.
[51] Perkins TK, Johnston OC. A review of diffusion and dispersion in porous media. Soc Petrol Eng J 1963;3(1):70–84. http://dx.doi.org/10.2118/480-PA.
[52] Medveď I, Černý R. Surface diffusion in porous media: a critical review. Microporous Mesoporous Mater 2011;142(2–3):405–22. http://dx.doi.org/10.1016/j.micromeso.2011.01.015.
[53] Caro J. Hierarchy in inorganic membranes. Chem Soc Rev 2016;45(12):3468–78. http://dx.doi.org/10.1039/c5cs00597c.
[54] Tridelta Siperm. Siperm R - technical data. 2019. URL, https://www.siperm.com/wp-content/uploads/2019/12/SIPERM-R-Technical-Data-englisch-1.pdf.
[55] B. Zhu, M. Duke, L. F. Dumée, A. Merenda, E. Des Ligneris, L. Kong, P. D. Hodgson, S. Gray, Short review on porous metal membranes-fabrication, commercial products, and applications, Membranes 8 (3). doi:10.3390/membranes8030083.
[56] Younglove BA. Thermophysical properties of fluids 1: argon, ethylene, parahydrogen, nitrogen, nitro trifluoride, and oxygen: supplement No, 1. American chemical Society and Bureau of Standards; 1982.
[57] Lemmon EW, Huber ML, Friend DG, Paulina C. Standardized equation for hydrogen gas densities for fuel consumption Applications1. SAE Technical Papers 2006. http://dx.doi.org/10.4271/2006-01-0434.
[58] Leachman JW, Jacobsen RT, Penoncello SG, Lemmon EW. Fundamental equations of state for parahydrogen, normal hydrogen, and orthohydrogen. J Phys Chem Ref Data 2009;38(3):721–48. http://dx.doi.org/10.1063/1.3160306.
[59] Lemmon EW, Huber ML, Leachman JW. Revised standardized equation for hydrogen gas densities for fuel consumption applications. J. Res Nat Inst Stand Techn 2008;113(6):341–50. http://dx.doi.org/10.6028/jres.113.028.
[60] Yusibani E, Woodfield PL, Shinzato K, Kohno M, Takata Y, Fujii M. Prediction of hydrogen gas viscosity at high pressure and high temperature. Netsu Bussei 2010;24(1):21–7. http://dx.doi.org/10.2963/jjtp.24.21.
[61] Hirschfelder JO, Curtiss CF, Bird RB. Molecular theory of gases and liquids, corr. print. with notes added. Edition, Structure of matter series. New York,NY: Wiley; 1964.
[62] Diller DE. Measurements of the viscosity of parahydrogen. J Chem Phys 1965;42(6):2089–100. http://dx.doi.org/10.1063/1.1696250.
[63] Assael MJ, Mixafendi S, Wakeham WA. The viscosity and thermal conductivity of normal hydrogen in the limit of zero density. J Phys Chem Ref Data 1986;15(4):1315–22. http://dx.doi.org/10.1063/1.555764.
[64] Kuwahara F, Kameyama Y, Yamashita S, Nakayama A. Numerical modeling of turbulent flow in porous media using a spatially periodic array. J Porous Media 1998;1(1):47–55. http://dx.doi.org/10.1615/JPorMedia.v1.i1.40.

[65] Amara M, Capatina D, Lizaik L. Coupling of Darcy–forchheimer and compressible Navier–Stokes equations with heat transfer. SIAM J Sci Comput 2009;31(2):1470–99. http://dx.doi.org/10.1137/070709517.
[66] Cimolin F, Discacciati M. Navier-Stokes/Forchheimer models for filtration through porous media. Appl Numer Math 2013;72:205–24. http://dx.doi.org/10.1016/j.apnum.2013.07.001.
[67] Soulaine C, Quintard M. On the use of a Darcy–Forchheimer like model for a macro-scale description of turbulence in porous media and its application to structured packings. Int J Heat Mass Tran 2014;74:88–100. http://dx.doi.org/10.1016/j.ijheatmasstransfer.2014.02.069.
[68] Li Z, Zhang H, Liu Y, McDonough JM. Implementation of compressible porous–fluid coupling method in an aerodynamics and aeroacoustics code part I: laminar flow. Appl Math Comput 2020;364:124682. http://dx.doi.org/10.1016/j.amc.2019.124682.
[69] Zhong W, Li X, Liu F, Tao G, Lu B, Kagawa T. Measurement and correlation of pressure drop characteristics for air flow through sintered metal porous media. Transport Porous Media 2014;101(1):53–67. http://dx.doi.org/10.1007/s11242-013-0230-2.
[70] Zhong W, Li X, Tao G, Kagawa T. Measurement and determination of friction characteristic of air flow through porous media. Metals 2015;5(1):336–49. http://dx.doi.org/10.3390/met5010336.
[71] Zhong W, Ji X, Li C, Fang J, Liu F. Determination of permeability and inertial coefficients of sintered metal porous media using an isothermal chamber. Appl Sci 2018;8(9):1670. http://dx.doi.org/10.3390/app8091670.
[72] Liao Y, Li X, Zhong W, Tao G, Liu H, Kagawa T. Experimental study of pressure drop-flow rate characteristics of heated tight porous materials. J Fluid Eng 2016;138(7):021702. http://dx.doi.org/10.1115/1.4032751.
[73] Najmi H, El-Tabach E, Chetehouna K, Gascoin N, Falempin F. Effect of flow configuration on Darcian and Forchheimer permeabilities determination in a porous composite tube. Int J Hydrogen Energy 2016;41(1):316–23. http://dx.doi.org/10.1016/j.ijhydene.2015.10.054.
[74] Forchheimer P. Wasserbewegung durch Boden. Z. Ver. Deutsch. Ing. 1901;45:1782–8.
[75] Ruth D, Ma H. On the derivation of the Forchheimer equation by means of the averaging theorem. Transport Porous Media 1992;7(3):255–64. http://dx.doi.org/10.1007/BF01063962.
[76] Whitaker S. The Forchheimer equation: a theoretical development. Transport Porous Media 1996;25(1):27–61. http://dx.doi.org/10.1007/BF00141261.
[77] Prachumchon S. A study of HDPE in high pressure of hydrogen gas—measurement of permeation parameters and fracture criteria. Ph.D. thesis. University of Nebraska-Lincoln; 2012.
[78] Yersak TA, Baker DR, Yanagisawa Y, Slavik S, Immel R, Mack-Gardner A, Herrmann M, Cai M. Predictive model for depressurization-induced blistering of type IV tank liners for hydrogen storage. Int J Hydrogen Energy 2017;42(48):28910–7. http://dx.doi.org/10.1016/j.ijhydene.2017.10.024.
[79] Pepin J, Lainé E, Grandidier J-C, Castagnet S, Blanc-vannet P, Papin P, Weber M. Determination of key parameters responsible for polymeric liner collapse in hyperbaric type IV hydrogen storage vessels. Int J Hydrogen Energy 2018;43(33):16386–99. http://dx.doi.org/10.1016/j.ijhydene.2018.06.177.
[80] Blanc-Vannet P, Papin P, Weber M, Renault P, Pepin J, Lainé E, Tantchou G, Castagnet S, Grandidier J-C. Sample scale testing method to prevent collapse of plastic liners in composite pressure vessels. Int J Hydrogen Energy 2019;44(17):8682–91. http://dx.doi.org/10.1016/j.ijhydene.2018.10.031.
[81] Blanc-Vannet P, Papin P, Weber M, Renault P, Pepin J, Lainé E, Tantchou G, Castagnet S, Grandidier J-C. Sample scale testing method to prevent collapse of plastic liners in composite pressure vessels. Int J Hydrogen Energy 2019;44(17):8682–91. http://dx.doi.org/10.1016/j.ijhydene.2018.10.031.
[82] Zhang M, Lv H, Kang H, Zhou W, Zhang C. A literature review of failure prediction and analysis methods for composite high-pressure hydrogen storage tanks. Int J Hydrogen Energy 2019;44(47):25777–99. http://dx.doi.org/10.1016/j.ijhydene.2019.08.001.
[83] Schrittesser B, Pinter G, Schwarz T, Kadar Z, Nagy T. Rapid Gas Decompression Performance of elastomers – a study of influencing testing parameters. Procedia Struct Integr 2016;2:1746–54. http://dx.doi.org/10.1016/j.prostr.2016.06.220.
[84] Balasooriya W, Schrittesser B, Karunakaran S, Schlögl S, Pinter G, Schwarz T, Kadar Z. Influence of thermo-oxidative ageing of HNBR in oil field applications. Macromol Symp 2017;373(1):1600093. http://dx.doi.org/10.1002/masy.201600093.
[85] Balasooriya W, Schrittesser B, Pinter G, Schwarz T. Induced material degradation of elastomers in harsh environments. Polym Test 2018;69:107–15. http://dx.doi.org/10.1016/j.polymertesting.2018.05.016.
[86] W. Balasooriya, B. Schrittesser, G. Pinter, T. Schwarz, L. Conzatti, The effect of the surface area of carbon black grades on HNBR in harsh environments, Polymers 11 (1). doi:10.3390/polym11010061.
[87] Agnelli S, Balasooriya W, Bignotti F, Schrittesser B. On the experimental measurement of fracture toughness in SENT rubber specimens. Polym Test 2020;87:106508. http://dx.doi.org/10.1016/j.polymertesting.2020.106508.
[88] Balasooriya W, Clute C, Schrittesser B, Pinter G. A review on applicability, limitations, and improvements of polymeric materials in high-pressure hydrogen gas atmospheres. Polym Rev 2021:1–36. http://dx.doi.org/10.1080/15583724.2021.1897997.
[89] Fujiwara H, Ono H, Ohyama K, Kasai M, Kaneko F, Nishimura S. Hydrogen permeation under high pressure conditions and the destruction of exposed polyethylene-property of polymeric materials for high-pressure hydrogen devices (2)-. Int J Hydrogen Energy 2021;46(21):11832–48. http://dx.doi.org/10.1016/j.ijhydene.2020.12.223.